Chapter 2

Recent Advances in the Theory of Quantum Tunneling for Luminescence Phenomena

Vasilis Pagonis

McDaniel College, Department of Physics
Westminster, MD 21157, USA
vpagonis@mcdaniel.edu

Although quantum tunneling models for luminescence phenomena have been developed over the last 40 years, interest in these models has been revived recently in two applied areas: dosimetry/dating applications, and development of luminescence nanomaterials with many practical applications. This chapter summarizes luminescence models for random distributions of electrons and positive ions in solids. Two different approaches have been developed within the context of these models. The first approach is a macroscopic point of view which uses differential equations, and this chapter reviews some of the available analytical equations in the literature. The second approach uses a microscopic description based on Monte Carlo simulations, which allow for spatial correlations between the charges. Monte Carlo methods have not been used extensively for this type of study. We will review recent work, and where applicable will compare the solutions of differential equations with the Monte Carlo simulations. Strengths and weaknesses of the two approaches will be presented. A third approach which bridges the first two approaches is also described, in which the differential equations are solved computationally using a Monte Carlo method. In the final part of this chapter we present simulations of luminescence phenomena for nanomaterials, with emphasis on the effect of crystal size on the experimentally measured luminescence signals.

2.1. Introduction

This chapter is a review of recent research on quantum tunneling models associated with luminescence phenomena in solids. More specifically, the models considered here are applicable to tunneling phenomena in systems of randomly located defects in a solid. There have been several efforts during the past 40 years to develop models for luminescence signals in solids originating in a random distribution of donor-acceptor pairs, especially in connection with kinetics of chemical reactions (see for example the book by Chen and Pagonis [1]; and references therein).

There are two major areas of applied research which provide the motivation for developing such models.

The first broad applied research area is in luminescence dosimetry and luminescence dating. From a dosimetry point of view, it is important to understand the tunneling mechanisms and the associated luminescence signals, with a view towards improving dosimetry and dating techniques. Quantum mechanical tunneling and the associated phenomena of "anomalous fading" and "long afterglow" of luminescence signals are now well established as dominant mechanisms in feldspars, apatites, rare earth doped materials and other important luminescent dosimetric materials (see for example the review paper, by Pagonis *et al.* [2]).

The second major experimental thrust for these types of models is for luminescence nanomaterials which find many practical applications. Recently luminescent materials consisting of nanoclusters with only a few atoms have attracted significant attention. The synthesis and characterization of such nanodosimetric materials has become an increasingly active research area, and it has been shown that their physical properties can be different from those of similar conventional microcrystalline phosphors (see for example Salah [3]; Sun and Sakka [4]; Eliyahu *et al.* [5]; and references therein). It has been suggested that traditional energy band models may not be applicable for some of these nanodosimetric materials, because of the existence of strong spatial correlations between traps and recombination centers. Such spatially correlated systems are also likely to be found in polycrystalline and low-dimensional structures, as well as in materials

which underwent high energy/high dose irradiations which create groups of large defects.

Two possible complementary modeling approaches have been used in the literature to simulate tunneling in random distributions of defects: a macroscopic description using differential equations, and a microscopic description based on Monte Carlo simulations. These two approaches are discussed in sections 2.2 and 2.3, together with an alternative third approach, in which the differential equations are solved computationally by using a different type of Monte Carlo method. Section 2.4 presents simulations of luminescence phenomena for nanomaterials, with emphasis on the effect of crystal size on the experimentally measured luminescence signals.

2.2. The macroscopic differential equation approach

In this section we will consider four different types of tunneling phenomena, all of which can be described with differential equations. Section 2.2.1 describes tunneling taking place from the ground state of the electron trap directly into the recombination center. Three approximate analytical equations are available in the literature, which are applicable under different relative concentrations of electrons and positive ions. Section 2.2.2 extends the work in section (2.2.1), to include the possibility of simultaneous irradiation and ground state tunneling of the material. Two analytical equations are available for such cases, which are applicable under the assumption that the concentration of electrons is much smaller than the corresponding concentration of positive ions.

Section 2.2.3 reviews extensive modeling work carried out during the past 10 years, which is based on tunneling taking place from the excited state of the electron trap. Several analytical equations are reviewed, which are again based on the assumption of the concentration of electrons being much smaller than the concentration of positive ions.

Figure 1 shows three previously proposed relatively simple models for luminescence signals in feldspars. Figure 1a and 1b show two ground state tunneling models considered by Tachiya and Mozumder

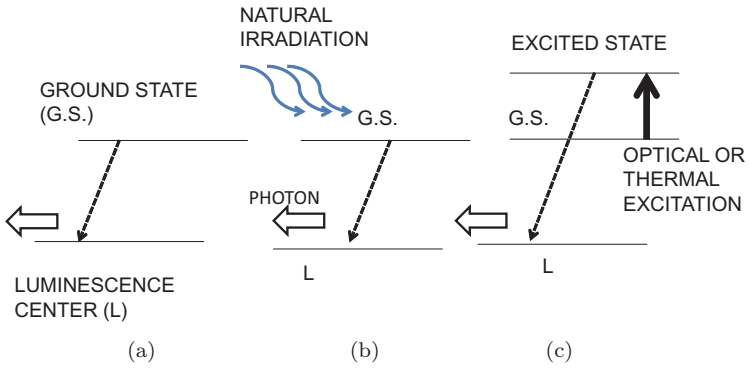

Fig. 1. Schematic depiction of the three luminescence models considered in this paper: (a) The ground state tunneling model. (b) The more general ground state tunneling model, in which anomalous fading and natural irradiation are taking place simultaneously. (c) The excited state tunneling model. (After Pagonis and Kitis [12]).

[6] and by Li and Li [7] respectively. Figure 1c shows an excited state tunneling model considered by Avouris and Morgan [8], Thioulouse and Chang [9], Jain *et al.* [10] and Kitis and Pagonis [11].

2.2.1. *Ground state tunneling models*

Several authors discussed the tunneling mechanism for a random distribution of donors and acceptors in a luminescent material, based on recombination taking place directly from the ground state of the system into the recombination center. The recombination of trapped charge is assumed to take place by quantum mechanical tunneling with a lifetime τ_{FADING} given by:

$$\tau_{FADING} = (1/s)\exp[\alpha r] \tag{1}$$

where α (m^{-1}) is the potential barrier penetration constant, r(m) is the separation distance between donor and acceptor and s (s^{-1}) is the attempt-to-tunnel frequency. The instantaneous concentration $n(r,t)$ of trapped electrons in the ground state depends on both the elapsed time t and on the separation distance r between donor and acceptor.

We will now consider three different cases, depending on the relative concentration of electrons/donors (n_o) and acceptors (m_o).

We first consider the situation where the concentration of electrons is much smaller than the concentration of acceptors, so that the system can be characterized by a *constant* number density of acceptors per unit volume ρ (m^{-3}). In such cases one can define a dimensionless distance parameter r', such that:

$$r' = (4\pi\rho/3)^{1/3} r \tag{2}$$

In addition one defines a *constant* dimensionless parameter ρ' proportional to ρ, by:

$$\rho' = (4\pi\rho/3)\alpha^{-3} \tag{3}$$

In order to maintain charge neutrality in this system of constant ρ, it is assumed that there is a large number of additional filled electron traps in the system, which do not participate in the tunneling process. This is a common situation in many dosimetric materials, in which several different types of electron traps are present. A second common assumption made in these tunneling models is that tunneling takes place only to the nearest neighbor in the system; this is known as the *nearest neighbor approximation*, and has been shown to be a reasonable approximation in most situations, except at very high charge densities. It can be shown from geometrical arguments that the nearest neighbor distribution of distances between electrons and acceptors is given by the following normalized distribution:

$$g_{NN}(r) = 4\pi\rho r^2 \exp[-(4\pi/3)\rho r^3] \tag{4}$$

In terms of the radius r' this equation becomes dimensionless:

$$g_{NN}(r') = 3(r')^2 \exp[-(r')^3] \tag{5}$$

As the tunneling process proceeds over time, the distribution of electrons in the ground state $n(r', t)$ varies with the distance parameter r' and with time t according to:

$$n(r', t) = 3n_o(r')^2 \exp[-(r')^3] \exp[-st \exp(-(\rho')^{-1/3} r')] \tag{6}$$

where n_o is the total initial number of donors in the system.

Figure 2a shows a plot of Eq. (6) at a time $t = 1000\,\mathrm{s}$ after the start of the tunneling process (dashed line). The solid line in Fig. 2a indicates the initial peak-shaped symmetric distribution $g_{NN}(r')$ obtained using Eq. (5), and the values of the parameters used in this simulation are typical for feldspars, $\rho' = 3 \times 10^{-6}$, $s = 3 \times 10^{15}\,\mathrm{s}^{-1}$. The dashed line in Fig. 2a represents the "moving tunneling front" in the tunneling process. The characteristic shape of this tunneling front is the product of the two functions appearing in Eq. (6), namely of the sharply rising double exponential function $\exp[-st\exp[-(\rho')^{-1/3}r']$, and of the symmetric distribution $g_{NN}(r')$.

The instantaneous total concentration of *remaining* carriers $n(t)$ is calculated by integrating Eq. (6) over all possible distances r':

$$n(t) = n_o \int_0^\infty 3(r')^2 \exp[-(r')^3] \exp[-t/\tau] dr' \tag{7}$$

In the approximate semi-analytical version of the model, one introduces a critical lifetime τ_c and a corresponding critical radius r'_c, which describe the behavior of the physical system. Geometrically, this approximation corresponds to replacing the dashed lines in Fig. 2a by a vertical line at $r' = r'_c$. Mathematically the value of the critical distance can be estimated from the *inflection point* of the double exponential function in Eq. (6) ([10, 12, 13]), and is given by:

$$r'_c = (\rho')^{1/3} \ln(st). \tag{8}$$

Using this approximation we can now evaluate the integral in Eq. (7), by replacing the exponential $\exp(-t/\tau)$ with a value of 0 for $t < \tau$, and with a value of 1 for $t > \tau$. By carrying out the integration we obtain the electron survival probability $S(t)$:

$$S(t) = n(t)/n_o = \exp[-\rho' \ln(st)^3] \tag{9}$$

A more accurate numerical approximation is obtained at all values of st by using the following slightly modified version of Eq. (9) (Kitis and Pagonis [11]):

$$S(t) = n(t)/n_o = \exp[-1.8\rho' \ln(st)^3] \tag{10}$$

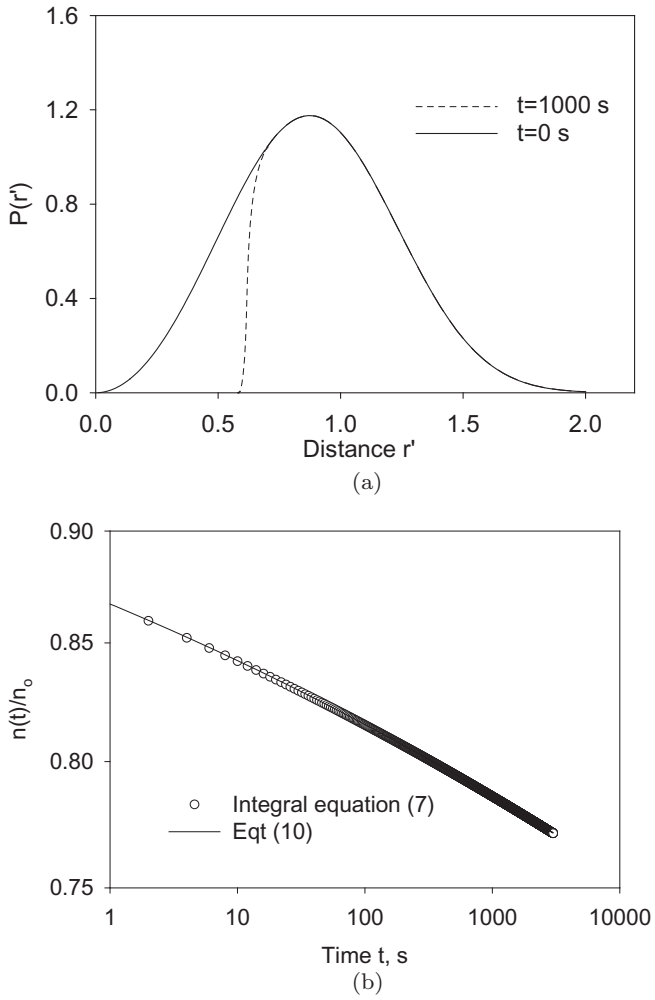

Fig. 2. (a) An example of the distribution of distances obtained using Eq. (6) as a function of the dimensionless distance r', and at a two times $t = 0\,\mathrm{s}$ (solid line), and at $t = 1000\,\mathrm{s}$ after the start of the tunneling process (dashed line). The critical radius corresponds to the approximation of replacing the dashed line by a vertical line. (b) Comparison of the concentration n(t) obtained by numerically integrating Eq. (7) over the possible range of values of distances, with the analytical expressions in Eq. (10). (After Pagonis *et al.* [13]).

Figure 2b shows a comparison of the concentration $n(t)$ obtained by numerically integrating Eq. (7) over the possible range of values of distances r', with the analytical expressions in Eq. (10), showing good agreement between the two approaches.

In summary, Eq. (7) is derived by assuming (a) a random distribution of defects (b) nearest neighbor interaction and (c) that the concentration of electrons is much smaller than the concentration of acceptors. Furthermore, Eq. (10) provides a good analytical approximation of Eq. (7).

Pagonis *et al.* [14] developed the following new analytical equation for the electron survival probability $S(t)$ for a random distribution of electrons and positive ions. This equation is derived on the assumption of *equal initial* concentrations $n_o = m_o$ of donors and acceptors correspondingly:

$$P(t) = 1/\{1 + (4\pi/3)n_o a^3[ln(st)]^3\} \tag{11}$$

Where $a = 1/\alpha$ (m^{-1}) is the tunneling length parameter, s (s^{-1}) is the tunneling frequency, and n_o, m_o are the initial equal concentrations of donors/acceptors at time $t = 0$.

Pagonis *et al.* [15] also considered cases of unequal initial concentrations of electrons and positive ions. They derived the following analytical equation for the electron survival probability:

$$P(t) = 1/\{-[n_o/\Delta m] + [m_o/\Delta m]\exp[(4\pi/3)\Delta m\ a^3[ln(st)]^3\} \tag{12}$$

Figure 3a shows graphs of Eq. (11) for different values of the dimensionless parameter $n'_o = n_o a^3$. Figure 3b shows graphs of Eq. (12) for different relative concentrations n_o/m_o and for $n_o < m_o$. In the limiting case where $n_o \ll m_o$, Eq. (12) becomes the same as Eq. (9) with $\rho' = 4\pi m_o a^3/3$.

2.2.2. *Irradiation and ground state tunneling*

Huntley and Lian [16] suggested an extension of the model in Fig. 1a, which uses a differential equation to describe simultaneous natural irradiation and anomalous fading effects on the luminescence of feldspars. Li and Li [7] applied the model of Huntley and Lian [16]

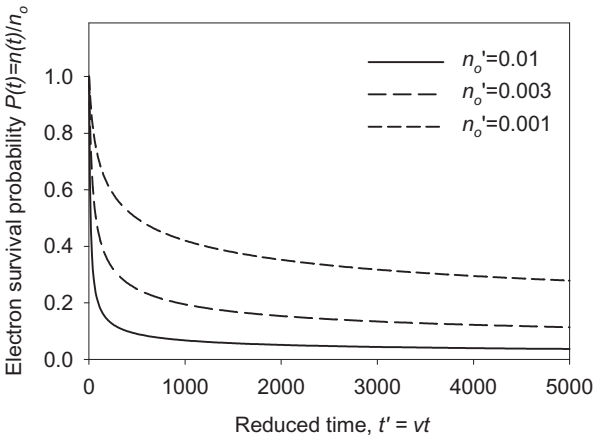

(a)

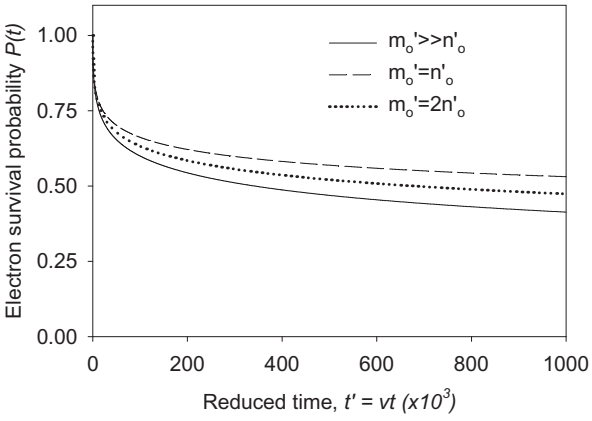

(b)

Fig. 3. (a) Plots of Eq. (11) for different values of the dimensionless parameter $n'_o = n_o a^3$. (b) Plots of Eq. (12) for different relative concentrations n_o/m_o and for $n_o < m_o$. (After Pagonis *et al.* [14]).

in an extensive experimental and modeling study of both laboratory-irradiated and naturally irradiated feldspars. These authors studied the decay of IRSL signals, the effects of anomalous fading on the shape of dose response curves (DRCs), the probability distribution of trap-to-center distance and the dependence of anomalous fading on the parameters of the model. They reported that the fading rates

depend strongly on the radiation dose previously received by the samples.

Li and Li [7] developed a single differential equation, whose solution for a constant distance r', is given by:

$$\frac{n(r')}{N(r')} = \frac{D_R\tau(r')}{D_R\tau + D_o}\left(1 - \exp\left[-\frac{D_R\tau(r') + D_o}{D_o\tau}t\right]\right) \qquad (13)$$

where D_R is the natural irradiation dose rate, D_o is the characteristic unfaded dose, $n(r')$ and $N(r')$ are the instantaneous and maximum possible concentrations of carriers corresponding to a given distance r', and the tunneling lifetime $\tau(r')$ is found from Eq. (1) as before. Using $t = D_n/D_R$ where D_n is the paleodose and by defining an effective characteristic dose $D'_o(r')$:

$$D'_0(r') = \frac{D_R\tau(r')D_o}{D_R\tau + D_o} \qquad (14)$$

Eq. (13) becomes:

$$\frac{n(r')}{N(r')} = \frac{D'_0}{D_o}\left(1 - \exp\left[-\frac{D_n}{D'_0}\right]\right) \qquad (15)$$

This is the saturating exponential function derived by Li and Li [7], which expresses how $n(r')$ fills up with the paleodose $D_n = D_R t$. Both the lifetime $\tau(r')$ and the effective characteristic dose constant $D'_o\,(r')$ depend on the distance r'. As time progresses, the probability distribution of distances r' for the system changes with the paleodose D_n according to the equation:

$$P_n(r') = \frac{P(r')n(r')}{N(r')} = 3(r')^2\exp(-(r')^3)\frac{D'_0}{D_o}\left(1 - e^{-\frac{D_n}{D'_0}}\right) \qquad (16)$$

where $P(r') = 3(r')^2\exp(-(r')^3$ is the unfaded nearest neighbor probability distribution function.

Figure 4a shows an example of the probability distribution function (PDF) $P_n\,(r')$ from Eq. (16), with the numerical values $\rho' = 3\times10^{-6}$, $s = 3\times10^{15}\,\mathrm{s}^{-1}$, $D_n = 500\,\mathrm{Gy}$, $D_R = 3\,\mathrm{Gy\ ka}^{-1}$ and $D_o = 538\,\mathrm{Gy}$. The solid curve in Fig. 4a represents the symmetric unfaded PDF, and the dashed curve represents the faded distribution $P_n\,(r')$. Physically this $P_n\,(r')$ function represents a "tunneling front"

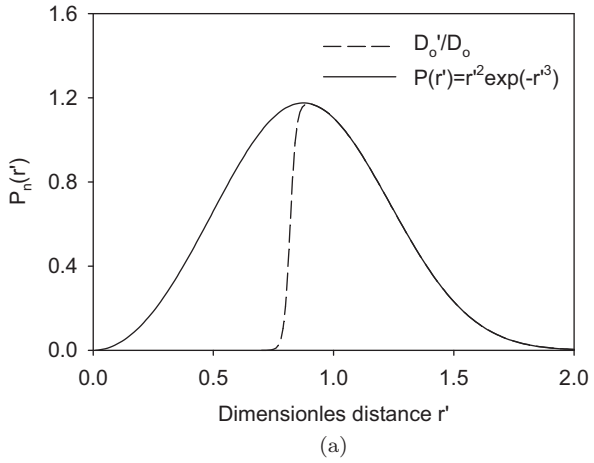

(a)

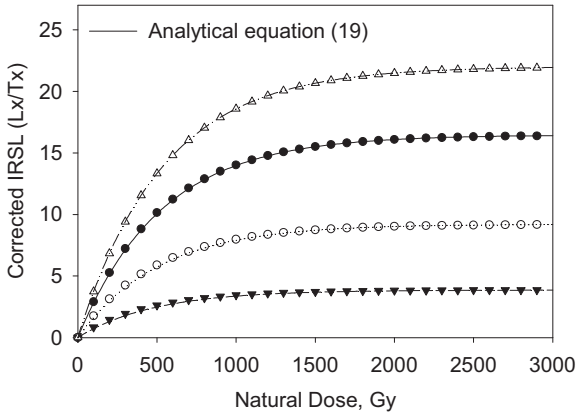

(b)

Fig. 4. (a) An example of the probability distribution $P_n(r')$ from Eq. (16). The solid line represents the symmetric unfaded PDF, and the dashed line represents the faded distribution $P_n(r')$, similar to the tunneling front shown in Fig. 2a for ground state tunneling. (b) Comparison of the DRC analytical Eq. (20) with the results obtained by the numerical integration of equations in the model. (After Pagonis and Kitis [12]).

which is mathematically similar to the front shown in Fig. 2a for ground state tunneling.

The modeling results of Li and Li [7] were expressed in terms of integral equations which require numerical integration over the

donor-acceptor distances in the model. Pagonis and Kitis [12] showed that the integral equations for DRCs in the model of Li and Li [7] can be replaced with analytical equations. These authors demonstrated the mathematical similarities between the two ground state tunneling models shown in Fig. 1ab, and introduced a critical radius approximation:

$$r_c' = (\rho')^{1/3} \ln\left(\frac{D_o s}{D_R}\right) \tag{17}$$

Using this value of the critical radius, one can now numerically evaluate the integrals in the work of Li and Li [7], to obtain this equation for the faded luminescence signal as a function of the natural dose D_n:

$$L_n(D_n) = \left(1 - \exp\left[-\frac{D_n}{D_0}\right]\right) M \exp\left\{-\rho' \ln\left[\frac{D_o s}{D_R}\right]^3\right\} \tag{18}$$

This is the desired analytical expression for the luminescence L_n as a function the natural dose D_n. For the unfaded signal, the corresponding expression is:

$$L_{unfaded} = M\left\{1 - \exp\left[-\frac{D_n}{D_0}\right]\right\} \tag{19}$$

Eqs. (18) and (19) are the important analytical equations for the faded and unfaded signals L_n and $L_{unfaded}$ and both equations are simple saturating exponentials of the natural dose D_n. The saturation level reached by the unfaded signal is equal to the total number of traps M, and the saturation level reached by the faded signal is equal to the second exponential term in Eq. (18). The ratio of the faded over the unfaded signal is then equal to $k = \exp(-\rho' \ln[(D_o s)/D_R]^3)$ and depends on the parameters ρ', s, D_R and D_o in the model. By using the previously stated values of these parameters, we obtain the fading ratio $k = 0.438 = 43.8\%$ of the original signal remaining in the sample, in agreement with experimental data.

Experimentally one usually measures a sensitivity corrected signal, by using the response of the material to a test dose. For a small

test dose of D_{test} the sensitivity corrected signal L/T is given by the analytical expression:

$$\frac{L_n}{T_n} = \frac{\left(1 - \exp\left\{-\frac{D_n}{D_0}\right\}\right) \exp\left\{-\rho' \ln\left[\frac{D_o s}{D}\right]^3\right\}}{\left(1 - \exp\left\{-\frac{D_{test}}{D_0}\right\}\right)} \tag{20}$$

Figure 4b compares the results from the DRC analytical Eq. (20) with the corresponding results obtained by the numerical integration of the equation in the model of Li and Li [7]. Very good agreement is seen at all values of the natural dose D_n.

Guralnik *et al.* [18] used a different approach based on a general-order kinetics model, to describe both the DRC's and the isothermal process in feldspars. They compared their model with experimental data for different materials by using a minimum of model parameters. These authors also compared their model with experimental data from a multi-elevated temperature post-IR IRSL (MET-pIRIR) dataset.

The empirical equation used by Guralnik *et al.* [18] to fit the DRCs is:

$$f(D) = a[1 - (1 + bcD)^{(-1/c)}] + d \tag{21}$$

where D is the dose and a, b, c, d are constants.

2.2.3. *Excited state tunneling*

Early modeling work was carried out by Avouris and Morgan [8] and Thioulouse *et al.* [9]. Jain *et al.* [10] presented a mathematical description of the model in Fig. 1c. The main assumptions of the model are the presence of a random distribution of electron-hole pairs, in which the concentration of holes (acceptors) is much larger than the concentration of electrons (donors). Thermal or optical excitation raises the electrons from the ground into the excited state of the system. Tunneling takes place from the excited state of the electron trap into the recombination center, and to the nearest neighbors only. Kitis and Pagonis [11] quantified the semi-analytical model of Jain *et al.* [10] by deriving analytical expressions for different experimental stimulation modes.

In additional work Pagonis *et al.* [13] examined the exact version of the model by Jain *et al.* [10] and showed that these equations for excited state tunneling are a direct generalization of the equations previously derived by Tachiya and Mozumder [6] for the case of ground state tunneling. These authors showed that the system of equations in Jain *et al.* [10] can be replaced with the following single differential equation:

$$\frac{dn(r',t)}{dt} = -\frac{As_{tun}}{B\exp[(\rho')^{-1/3}r']}n(r',t) \tag{22}$$

where $n(r',t)$ represents the concentration of electrons in the ground state, and n_o is the total initial number of donors in the system, as in the previous sections. In addition, A is the rate of excitation of the electron from the ground into its excited state, B is the transition rate from the excited into the ground state, and s_{tun} is the frequency factor characterizing the tunneling process taking place from the excited state of the system. In previous modeling work by Jain *et al.* [10] and Kitis and Pagonis [11], it was assumed for simplicity in the model that $s_{tun} = B$, which led to a simplified form of Eq. (22). However, from a physical point of view, there is no relationship between the two parameters s_{tun} and B, so one should not assume that they are equal.

The total remaining number of electrons in the ground state at time t is given by:

$$n(t) = \int_0^\infty 3n_0(r')^2\exp[-(r')^3]\exp\left[-\frac{s_{tun}}{B\exp[(\rho')^{-1/3}r']}\int_0^t Adt'\right]dr' \tag{23}$$

Eq. (23) allows a numerical calculation of $n(t)$, by numerical integration.

The value of the parameter A in the above equation depends on the stimulation mode used in the experiments. In the case of continuous wave infrared stimulated (CW-IRSL) experiments, the parameter A represents the constant rate of infrared excitation A_{IR},

and the integral in this equation can be replaced by $A_{IR}t$, where t is the time elapsed from the beginning of the IR-excitation. In an isothermal decay experiment, the temperature T_{ISOTH} of the sample is kept constant and the parameter A is replaced by the constant rate of thermal excitation $A_{ISOTH} = s_{th}\exp(-E/k_BT_{ISOTH})$, where E is the thermal activation energy and s_{th} is the pre-exponential factor for the thermal excitation process, which is proportional to the lattice vibration frequency. In this case the integral can be replaced by $A_{ISOTH}t$, where t is the elapsed time from the isothermal experiment. In a TL experiment, the sample is heated with a linear heating rate β, from a starting temperature T_o up to a high temperature around 500°C. In this case parameter A is replaced by time-dependent probability of thermal excitation $A_{TL} = s_{th}\exp[-E/kT(t)]$ where k is the Boltzmann constant and the integral can be approximated to any desired degree of accuracy by using the exponential integral function $E_i(T)$ (Chen and Pagonis [1]). During linearly modulated IRSL (LM-IRSL) experiments, the probability of optical excitation is varied linearly with time in the form $A = bt/T$, where T = total excitation period and b is an experimental constant. The integral can now be replaced by $bt^2/2T$, where t is the time elapsed in the LM-IRSL excitation.

The analytical solution of Eq. (23) for excited state tunneling was developed by Kitis and Pagonis [11]:

$$n(t) = n_o\exp[-\rho' F(t)^3] \tag{24}$$

$$F(t) = \ln\left(1 + 1.8\int_0^t A dt'\right) \tag{25}$$

$$L(t) = -\frac{dn}{dt} = \frac{AF(t)^2\exp[-\rho'[F(t)]^3]}{1 + 1.8\int_0^t A dt'} \tag{26}$$

Where $L(t)$ represent the luminescence intensity observed during these different types of experiments. Figure 5 shows examples of 2 different types of experimental data, which was analyzed using Eqs. (24)–(26).

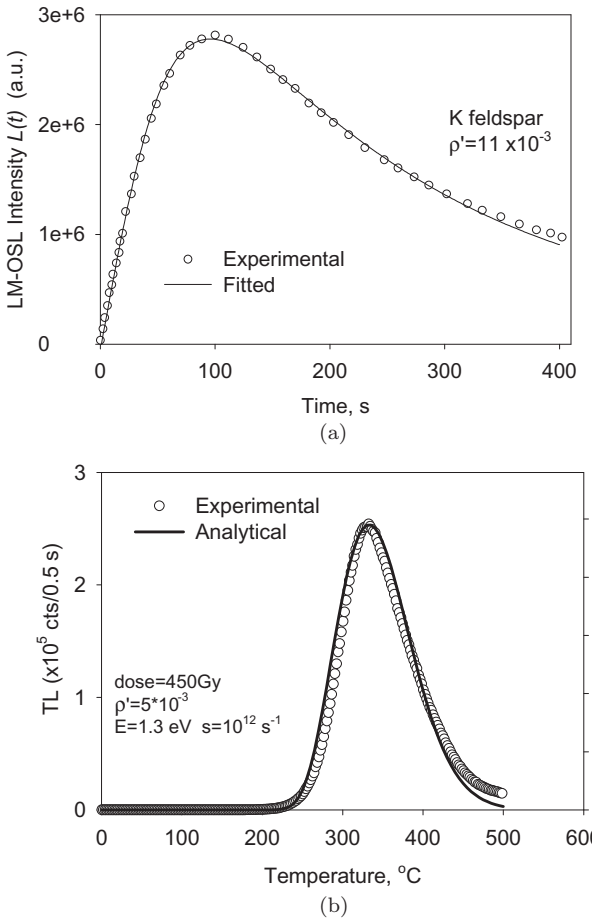

Fig. 5. (a) LM-OSL data (b) TL data analyzed using Eqs. (24)–(26) in the text (After Kitis and Pagonis [11]).

2.3. The microscopic Monte Carlo approach

The Monte Carlo simulations can provide valuable insight into the various factors which affect the luminescence mechanism in these materials. The advantages of using a Monte Carlo method, as opposed to the differential approach, are (Pagonis and Kulp, [18]):

- Monte Carlo methods are fast, efficient and avoid numerical integrations required in the differential equation approach.

- MC methods can be used to produce accurate results in cases of low stimulation probability, in which it is known that the analytical equations of Kitis and Pagonis [11] fail.
- They can be used for both freshly irradiated samples, and for irradiated samples which underwent thermal or optical pre-treatments.
- They can also be used to describe time-resolved experiments based on Mott hopping processes.

Section 2.3.1 summarizes earlier Monte Carlo work on luminescence clusters, and reviews the recent work by Pagonis *et al.* [19] which is based on the general one trap (GOT) model. Sections 2.3.2 describes the recent work by Pagonis and Kulp [17], who simulated the loss of charge due to ground state tunneling, as well as the charge creation by natural irradiation of the samples.

Section 2.3.3 considers the simultaneous processes of irradiation and charge loss due to ground state tunneling, and compares the Monte Carlo simulations with analytical expressions in the literature. Section 2.3.4 presents a hybrid Monte Carlo method, which is based on the solution of differential equations for a finite number of charge carriers in a solid.

2.3.1. *Monte Carlo under QE conditions*

Early Monte-Carlo methods for the study of thermoluminescence (TL) were presented in the papers by Kulkarni [20], Mandowski [21–23] and Mandowski and Świątek ([24–27]). These authors suggested that usually the number of carriers in a sample is large and the differential equations used in traditional kinetic models describe the system properly. However, in some solids one must consider clusters of traps as separate systems, since the continuous differential equations are not valid. Typically the Monte Carlo calculations are performed with the total population of carriers simultaneously, and in each step of the Monte-Carlo simulation one finds the lowest transition time for all possible transitions, and this is the only transition which is executed. These studies of TL showed that spatially correlated effects become prominent for low concentrations of thermally disconnected traps and for high recombination situations.

In additional Monte Carlo applications in luminescence, Pagonis and Kitis [28] studied several popular luminescence models using random combinations of variables, while Pagonis *et al.* [29] applied the same technique in simulating several dating protocols for quartz. Adamiec *et al.* ([30, 31]) used a method of random variation of kinetic parameters to develop a genetic algorithm for luminescence models.

The above mentioned studies have focused on the properties of TL glow curves using Monte Carlo simulations. Pagonis *et al.* [19] used a simple technique based on the general one trap (GOT) model of luminescence, and obtained physical insight into the nature of the simulated multi-peak TL and linearly modulated OSL signals (LM-OSL), by varying the parameters in the model. The physical picture in the simple model of these authors is that the system consists of many independent clusters of electron-hole pairs. Electrons are released from the traps and into the conduction band by either thermal or optical stimulation. Subsequently they are either recombined radiatively or are retrapped, with both retrapping and recombination taking place *within the same cluster*. The simplified model is based on the differential equation:

$$I_{TL}(t) = -\frac{dn}{dt} = \frac{n^2 p(t)}{(N-n)r + n} \tag{27}$$

where N (cm^{-3}) is the total concentration of dosimetric traps, $n(\mathrm{cm}^{-3})$ is the concentration of filled dosimetric traps. r is the ratio of the capture coefficients A_n and A_m ($\mathrm{cm}^3\mathrm{s}^{-1}$) of the trap and recombination center respectively, and $p(t)$ is the experimental rate of excitation of the electrons in the trap. In the case of TL, the rate of thermal excitation is $p(T) = s\exp(-E/kT)$ where E (eV) and s (s^{-1}) represent the thermal activation energy and the frequency factor of the dosimetric trap, correspondingly, T is the absolute temperature and k the Boltzmann constant. The initial concentrations of filled traps at time $t = 0$ are denoted by the symbol n_0, and a linear heating rate is assumed during the TL experiment. In the case of continuous-wave OSL signals (CW-OSL), $p(t) = \lambda(\mathrm{s}^{-1})$ is the constant rate for optical excitation and in the case of LM-OSL experiments, $p(t) = bt$, where b is a parameter which depends on

the experimental conditions and on the optical cross section for the traps under consideration. In the "brute force" Monte Carlo method presented by Pagonis *et al.* [19], this becomes a difference equation for the discrete variable n:

$$\Delta n = -\frac{n^2 p(t)}{(N-n)r + n}\Delta t \tag{28}$$

The dimensionless time-dependent probability P for an electron to recombine within a time interval Δt is $P = p(t)Dt$, and a suitable value of Δt is chosen so that $P \ll 1$. A random number r uniformly distributed in the unit interval $0 \leq r < 1$ is generated; if $r \leq P$ the recombination takes place, otherwise it does not. The value of the remaining electrons n is updated at the end of each time interval Δt, and the process is continued until there are no electrons left. These authors used local variables to describe the internal structure of each cluster, and global variables which describe the whole group of clusters. A double iterative loop is used, with the inner loop simulating a single cluster using local variables, and with the outer loop simulating the whole group of clusters using global variables. A third iterative loop advances the time t by increments of Δt, simulating the thermal/optical stimulation of the system.

Figure 6a shows a typical simulated system of small trap clusters, in which there are 4 traps in each cluster (shown as both open and solid circles), with only 3 of them being initially filled (shown as solid circles). One ensures the charge balance in the system, by assuming the existence of an equal number of 4 luminescence centers (shown as both open and solid stars), 3 of which have been activated (shown as solid stars). Figure 6b shows the results of a Monte Carlo simulation for the TL signal, with the kinetic parameters $s = 10^{10}\,\mathrm{s}^{-1}$, $E = 0.9\,\mathrm{eV}$, a linear heating rate $1K/s$ and the retrapping ratio $r = A_n/A_m = 10^3$. The system consists of two initially filled traps per cluster, and a large number of $n_o = 2 \times 10^5$ initially filled traps. The TL glow curve in Fig. 6b consists of 2 peaks; this is consistent with the work of Mandowski and Świątek [26], who showed that the number of constituent TL peaks should be equal to the number of filled traps per cluster.

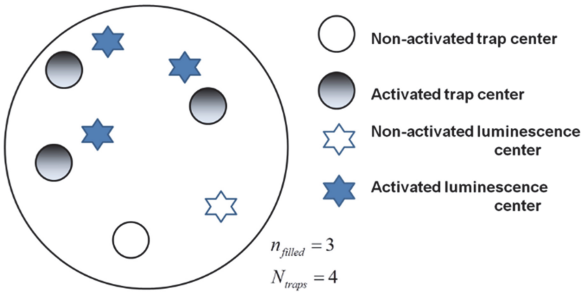

(a)

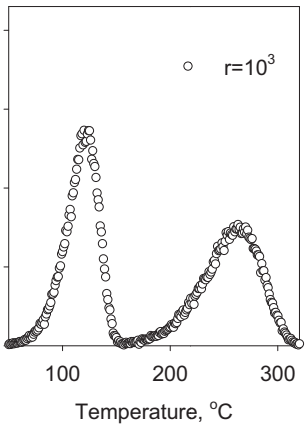

(b)

Fig. 6. (a) The model of Pagonis *et al.* [19] based on the GOT model (b) Simulated TL glow curve based on the model shown in (a).

Pagonis and Chen [32] applied the same simple Monte Carlo method to the semi-analytical version of the model by Jain *et al.* [10], in which the system of simultaneous differential equations can be approximated to a very good precision by the difference equation.

$$\Delta n = -3\rho'^{1/3} Az \exp\left[\left(\frac{1}{\rho'}\ln\frac{n_{filled}}{n}\right)^{1/3}\right]\left(\ln\frac{n_{filled}}{n}\right)^{2/3} n\Delta t \tag{29}$$

where $z = 1.8$, n_{filled} is the local parameter for the initially filled traps in the cluster, and the rest of the parameters were defined previously.

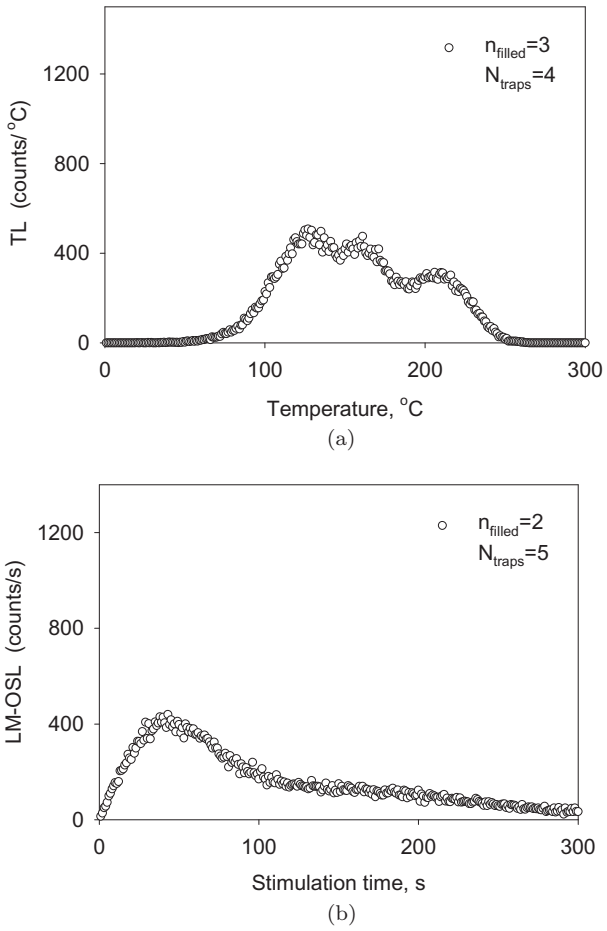

Fig. 7. (a) Simulation of TL glow curve (b) Simulation of LM-OSL curve (from Pagonis and Chen [32]).

Figures 7a and 7b show typical results from Eq. (29), for a simulated TL and LM-OSL experiment correspondingly.

2.3.2. *Monte Carlo simulations of ground state tunneling*

Larsen *et al.* [33] presented a numerical Monte Carlo model that simulated the processes of charge loss, charge creation and charge

recombination in feldspar. Their main assumptions were that the number density of electrons and holes are equal at all times, and that nearest neighbor interactions take place. The focus of their study was to reproduce the experimentally observed values of the well-known g-factor describing anomalous fading effects. These authors were not able to get reliable results for bulk crystals, and obtained good agreement with experiment only when they assumed that the material consisted of small nanocrystals, and that charge carriers were allowed to recombine only within these smaller volumes.

Pagonis and Kulp [17] presented a different version of the model by Larsen *et al.* [33], in which the number density of acceptors far exceeds that of donors. The new version of the model was used to simulate the loss of charge due to ground state tunneling, as well as the charge creation by natural irradiation of the samples. The results from the model compared well with the analytical equations (24–26) presented in the previous subsection. The simulations can describe the loss of charge on a wide variety of time scales, from microseconds to thousands of years. The effect of crystal size, charge carrier density, natural irradiation dose rate and total number of charge carriers were studied in a quantitative manner.

Figure 8 shows typical simulation results obtain by Pagonis and Kulp [17]. During the simulation each of the electrons in the volume is examined, and the distances of this electron from all holes are calculated. The minimum distance r_{MIN} to the nearest neighbor is found, and the Monte Carlo algorithm generates $i = 1 \ldots n_{DONORS}$ possible random fading times t^i_{FADING} given by:

$$t^i_{FADING} = -s^{-1} \exp(\alpha\, r_{MIN}) \ln(1 - P_i) \tag{30}$$

where P_i is a random number between 0 and 1, representing the probability of recombination for each surviving electron. These possible times t^i_{FADING} depend on the tunneling frequency s, on the barrier penetration parameter α, and on the instantaneous distribution of distances r_{MIN} in the system. Close-by pairs are more likely to recombine first, and further away pairs are likely to recombine later. Only the event corresponding to the shortest of all

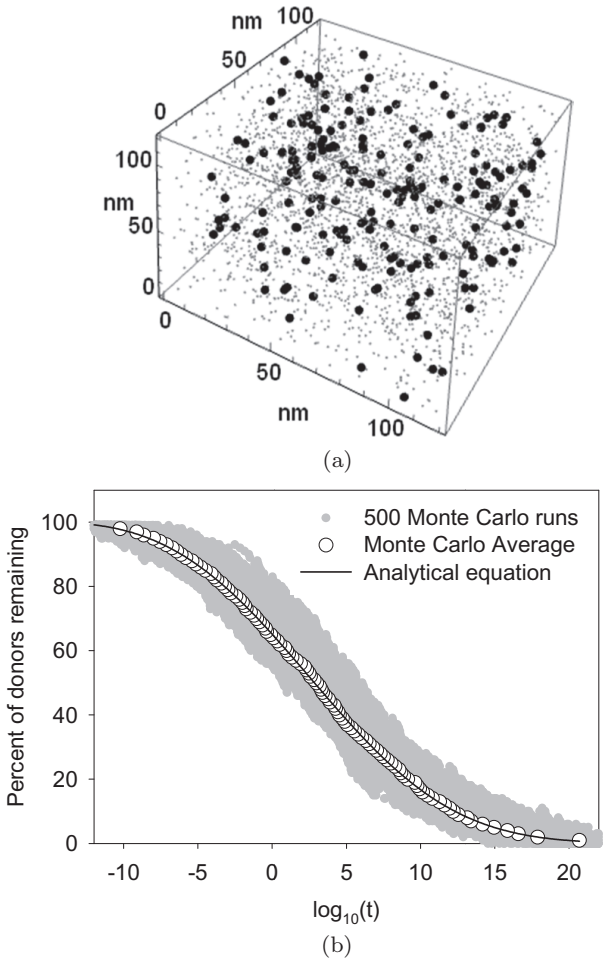

Fig. 8. (a) A cube containing random distributions of electrons and positive ions (b) Monte Carlo simulation of the charge loss in the distribution shown in (a) (After Pagonis and Kulp [17]).

the possible times in Eq. (30) happens, i.e. the donor-acceptor pair corresponding to this shortest time is allowed to recombine. After this pair is removed from the system in the simulation, the distances between each donor and each acceptor are re-evaluated, and the minimum t^i_{FADING} time is used to update the total time elapsed from

the beginning of the simulation. This process is repeated until there are no more donors left in the system.

The Monte Carlo simulations average the results from 500 such random cubes of the same size shown in Fig. 8a, with typical results shown in Fig. 8b. The parameters used for the simulation in Fig. 8 are $\rho' = 10^{-5}$, $s = 3 \times 10^{15}\,\mathrm{s}^{-1}$, $n_{DONORS} = 100$ and $n_{ACCEPTORS} = 1222$, the potential barrier penetration constant $\alpha = 4 \times 10^{9}\,\mathrm{m}^{-1}$ and the size of the cube $d = 200\,\mathrm{nm}$. The solid line in Fig. 8b represents the analytical Eq. (10) for the loss of charge due to ground state tunneling. Very good agreement is obtained between the analytical equation and the results of the Monte Carlo simulation. Finally, Pagonis and Kulp [17] extended their version of the model to describe luminescence signals originating in the nearest neighbor hopping mechanism in feldspars, and compared with experimental data from time-resolved infrared stimulated luminescence (TR-IRSL) in these materials.

2.3.3. *Monte Carlo simulations of simultaneous irradiation and tunneling*

Pagonis and Kulp [17] simulated the simultaneous processes of charge loss by tunneling, and charge creation by irradiation in nature, and compared the results of the Monte Carlo simulations with previously derived analytical equations. The simulations were compared with analytical expressions over a wide variety of time scales, from microseconds to thousands of years. These authors were able to produce quantitative agreement of the Monte Carlo model with experimental data for both bulk and nano-sized crystals. They studied quantitatively the influence of various parameters in the model, such as the crystal size, charge carrier density, natural irradiation dose rate and total number of charge carriers.

Figure 9a shows the results of the acceptor density on the loss of charge due to tunneling. Figure 9b shows the dose response of a feldspar sample under the simultaneous effect of tunneling and natural irradiation. The solid line represents the analytical Eq. (18) derived by Pagonis and Kitis [12].

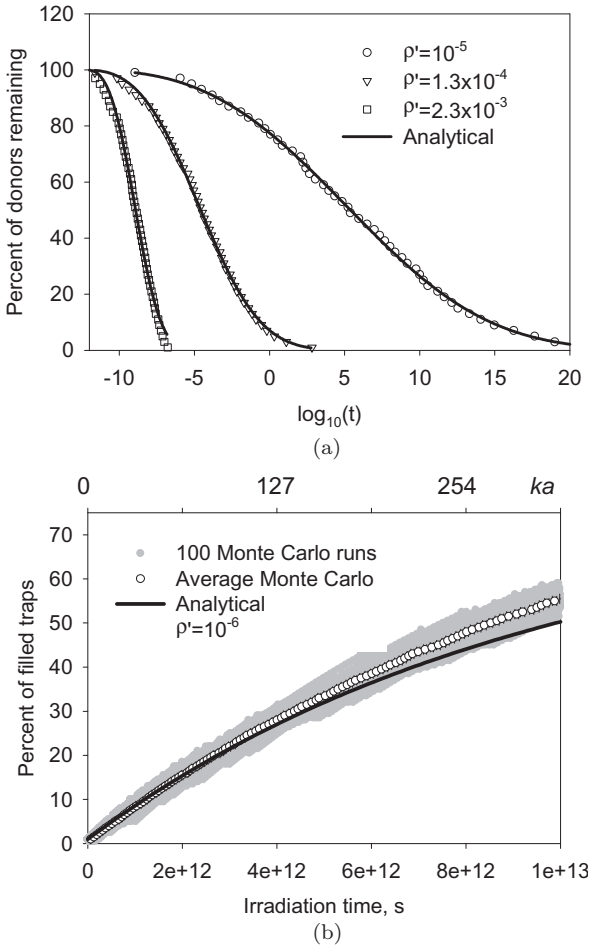

Fig. 9. (a) Effect of density on the loss of charge by tunneling (b) dose response under simultaneous irradiation and tunneling (After Pagonis and Kitis [12]).

2.3.4. *Monte Carlo simulations of tunneling from the excited state*

In this section we present a different Monte Carlo technique which can be used to study tunneling from the excited state of a trap, as shown schematically in Fig. 1c. This alternative computational approach has the advantage that it can be applied to any of the different situations presented in sections 2.2 and 2.3. Furthermore,

this method can be used for both freshly irradiated samples, and for irradiated samples which underwent thermal or optical pre-treatments before measurement of their luminescence signal.

The method is based on Eq. (22), which is written as a difference equation for the discrete variable $n(r', t)$ characterizing the number of electrons in the material:

$$\Delta n(r', t) = -\frac{As_{tun}}{B \exp[(\rho')^{-1/3} r']} n(r', t) \Delta t. \tag{31}$$

The total number $n(t)$ of remaining electrons at time t, and the luminescence intensity $I(t)$ are evaluated from the finite sums:

$$n(t) = \sum_{r'=0}^{2} n(r', t) \Delta r' \tag{32}$$

$$L(t) = -\sum_{r'=0}^{2} \frac{\Delta n(r', t)}{\Delta t} \Delta r'. \tag{33}$$

For pretreated samples one can approximate the nearest neighbor distribution with a *truncated* distribution function which extends from a minimum critical radius r'_c up to infinity (Pagonis *et al.* [13]; Jain *et al.* [34]). This critical radius can be treated as an adjustable modeling parameter when fitting experimental data. For such samples the summations in Eqs. (32)–(33) start at $r = r'_c$, instead of starting at $r' = 0$. In these equations $\Delta r'$ is an appropriate distance interval, e.g. $\Delta r' = 0.02$. The overall evolution of the system must be followed for *both* the time variable t, and for each value of the dimensionless distance r', by using two iterative loops. The inner loop is executed using a time variable t, and for a constant value of the distance parameter r'. The outer loop repeats the inside loop for all possible discrete values of the parameter $r' = r' + \Delta r'$. At time $t = 0$ there are n_o filled traps, and the distribution of nearest neighbors is given by the peak shaped function. The rate P for an electron to recombine radiatively within the time interval Δt and for certain distance r' is given by the function on the right hand side of Eq. (31). By following the same method as in Pagonis *et al.* [19], and Pagonis and Chen [32], one chooses a suitable value

of Δt so that $P\Delta t \ll 1$, and a random number r is generated, which is uniformly distributed in the unit interval $0 \leq r < 1$. If $r \leq P$ the electron recombines radiatively, otherwise it does not; all non-recombined remaining electrons in the system are tested in this manner during each time interval Δt, and at the end of each time interval Δt, the program stores the values of $n(r', t)$ and $\Delta n(r', t)/\Delta t$. This process is now repeated for the next value of the

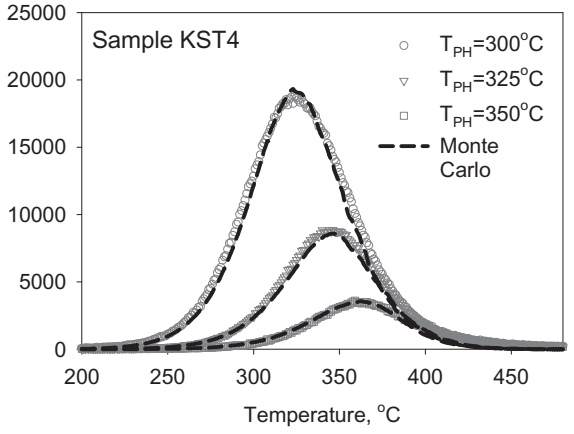

(a)

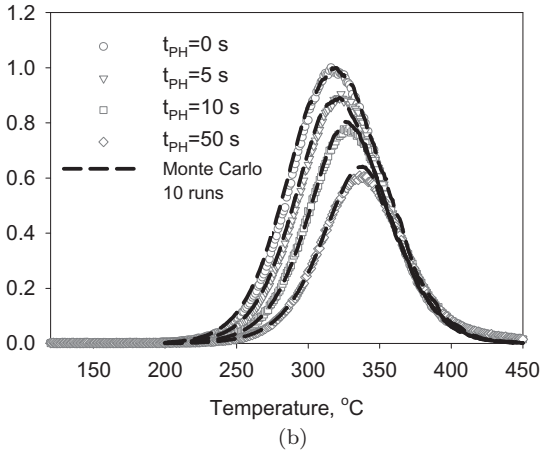

(b)

Fig. 10. (a) Comparison of model with experimental TL glow curves of irradiated sample preheated at different temperatures (b) Same as (a), for a sample preheated at different times for a fixed preheating temperature (After Polymeris *et al.* [35]).

distance r' in the outer software loop. Finally the contributions from all distances r' are added according to Eqs. (32) and (33), resulting in the simultaneous evaluation of the discrete-value functions $n(t)$ and $L(t)$. Both iterative loops are executed until there are no particles left in the system. Figure 10 shows how the results of this method compare with experimental data.

2.4. Monte Carlo simulations of luminescence phenomena in nanodosimetric materials: ground state tunneling

In this section we present simulations of luminescence phenomena for nanomaterials based on ground state tunneling, with emphasis on the effect of crystal size on the experimentally measured luminescence signals.

Pagonis *et al.* [15] simulated the effect of crystal size on quantum tunneling phenomena in nanocrystals, based on the assumption of a random distribution of electrons and positive ions. They found a rather complex behavior of such random distributions, which is determined by three characteristic lengths: the radius of the crystal R, the tunneling length a, and the initial average distance $\langle d \rangle$ between electrons and positive ions (which is directly related to the density of charges in the material). Two different cases were examined, depending on the relative concentrations of electrons and ions. In the first case described in section 2.4.1, the concentration of electrons was assumed to be much smaller than the concentration of positive ions, and an analytical equation is available to describe the effect of varying crystal size. In the second situation presented in section 2.4.2, the concentrations of electrons and positive ions were equal at all times, and no analytical equation is available to describe the process. As a consequence, crystal size effects in this situation must be simulated using Monte Carlo techniques.

2.4.1. *Case #1: Concentration of electrons much smaller than concentration of positive ions*

When the concentration of positive ions ρ far exceeds the concentration of electrons in the system, then ρ can be considered

to stay almost constant during the tunneling process. Tachiya and Mozumder [6] developed the following analytical equation to describe the electron survival probability $P(t)$ in a spherical random distribution of electrons and positive ions with radius R:

$$P(t) = \left[\frac{1}{(4/3\pi R^3)}\int_0^R \exp\left[\frac{-t}{\tau_{FADING}(r)}\right] 4\pi r^2 dr\right]^{\rho(4/3\pi R^3)}, \quad (34)$$

where the lifetime τ_{FADING} is given by Eq. (1). It is noted that Eq. (34) has been available for more than 40 years in the literature, but was used only recently to describe crystal size effects on tunneling phenomena.

In the limit of bulk large crystals $R \to \infty$, Tachiya and Mozumder [6] showed that Eq. (34) has the following analytical expression:

$$P(t) = \exp\left[-\rho\left(\frac{4}{3}\pi a^3\right) g(st)\right], \quad (35a)$$

$$g(st) = \ln(st)^3 + 1.7316\ln(st)^2 + 5.9343\ln(st) + 5.4449. \quad (35b)$$

Pagonis *et al.* [15] studied the behavior of Eq. (34) as a function of the radius R, and with a constant density of positive ions ρ, and found two opposite behaviors as a function of the crystal size. When the tunneling length a is much smaller than both R and $\langle d\rangle$, the analytical equations show that smaller crystals exhibit a faster tunneling recombination rate, as shown in Fig. 11a.

However, when the tunneling length a is of the same order of magnitude as both R and $\langle d\rangle$, the opposite effect is observed in Fig. 11b, with smaller crystals exhibiting a slower tunneling recombination rate. As the crystal size increases, the rate of tunneling in both cases reaches the limit expected for bulk materials, given by Eq. (35).

In the second situation presented in section 2.4.2, the concentrations of electrons and positive ions were equal at all times, and no analytical equation is available to describe the process. As a consequence, crystal size effects in this situation must be simulated using Monte Carlo techniques.

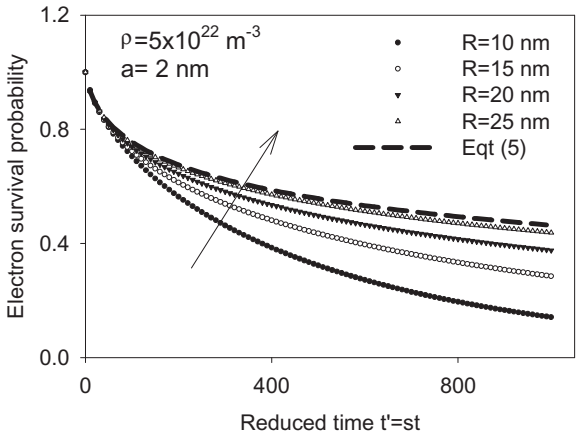

(a)

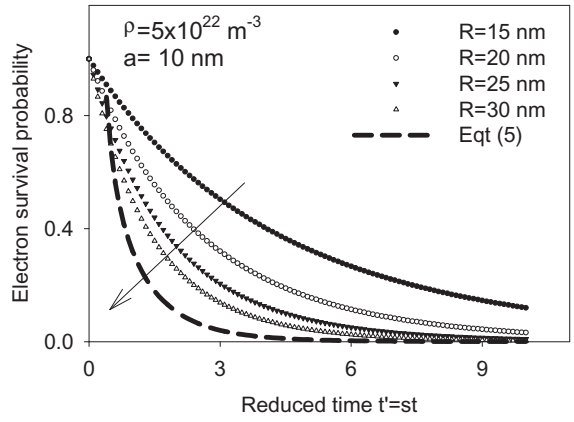

(b)

Fig. 11. (a) The results of integrating Eq. (34) numerically for a positive ion density $\rho = 5 \times 10^{22}\,\mathrm{m}^{-3}$, tunneling length $a = 2\,\mathrm{nm}$, and for crystal sizes $R = 10 - 25\,\mathrm{nm}$. The dashed line shows the limit described by the analytical equation (24). (b) Same as (a), for a longer tunneling length $a = 10\,\mathrm{nm}$, and for a radius in the range $R = 15$–$30\,\mathrm{nm}$. (After Pagonis *et al.* [15]).

2.4.2. *Case #2: Equal concentrations of electrons and positive ions at all times*

Pagonis *et al.* [15] discussed the situation when the concentrations of electrons and positive ions are equal at all times. In this case crystal size effects must be simulated using Monte Carlo techniques. These

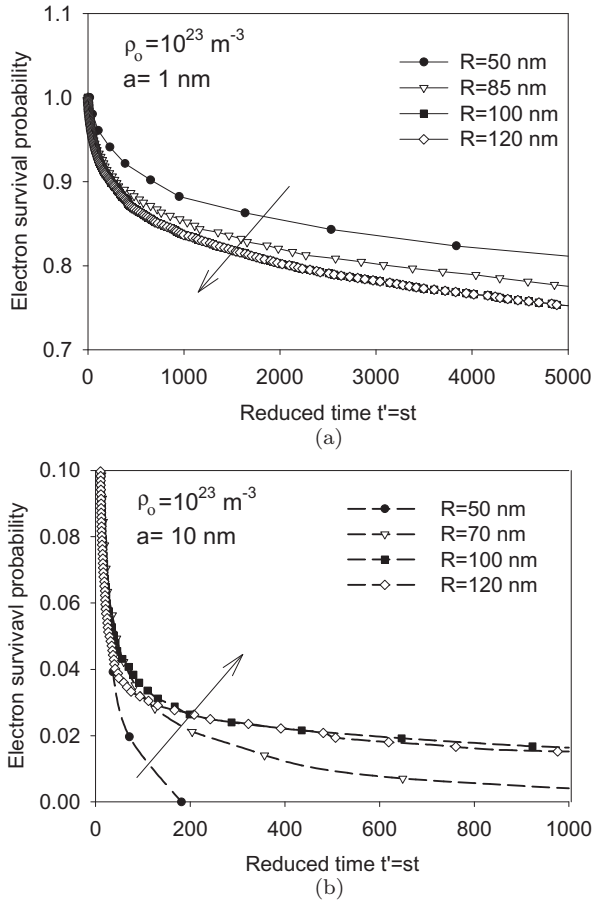

Fig. 12. (a) The results of Monte Carlo simulations of a spherical distribution, for an *initial* positive ion density $\rho = 10^{23}\,\mathrm{m}^{-3}$, tunneling length $a = 1\,\mathrm{nm}$, and for crystal sizes $R = 50 - 120\,\mathrm{nm}$. (b) Same as (a), for a longer tunneling length $a = 10\,\mathrm{nm}$. (After Pagonis *et al.* [15]).

authors employed the Monte Carlo method described in Pagonis and Kulp [17], and examples of the results of their simulations are shown in Fig. 12.

The Monte Carlo simulations of Figs. 12ab show the same effect of crystal size on the tunneling rate as the results of the analytical Eq. (34) shown in Fig. 11.

Pagonis *et al.* [15] also studied the effect of sample temperature, by extending the Monte Carlo simulations to include thermal characteristics of the defects. By following the suggestion by Larsen *et al.* [33], these authors included the thermal time constant $\tau_{THERMAL} = (1/s)\exp(E/kT)$, which is assumed to be constant and the same for all traps. This Arrhenius-type thermal time constant $\tau_{THERMAL}$ is

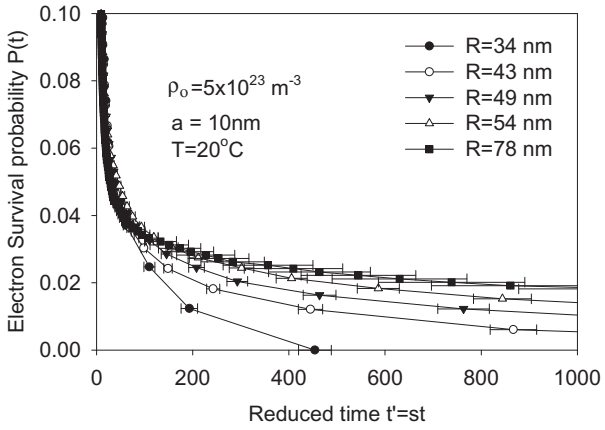

(a)

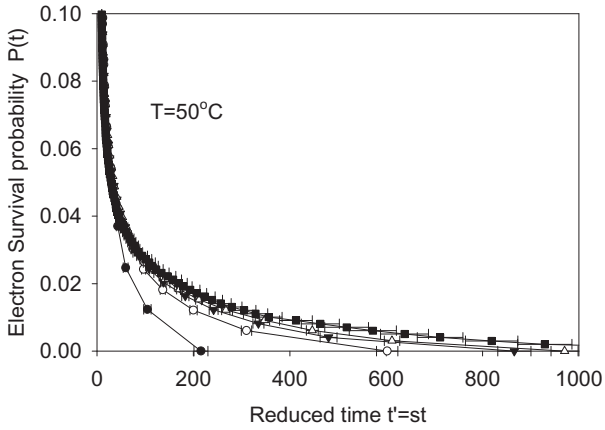

(b)

Fig. 13. (a) The results of Monte Carlo simulations of a spherical distribution, for an *initial* positive ion density $\rho = 10^{23}\,\mathrm{m}^{-3}$, tunneling length $a = 1\,\mathrm{nm}$, and for crystal sizes $R = 50$–$120\,\mathrm{nm}$. (b) Same as (a), for a longer tunneling length $a = 10\,\mathrm{nm}$. (After Pagonis *et al.* [15]).

characterized by the thermal activation energy E and the thermal frequency factor s, k is the Boltzmann constant and T is the temperature of the sample.

The results of the simulations are shown in Fig. 13 with the parameters $E = 1\,\text{eV}$, $s = 10^{12}\,s^{-1}$, initial charge density $\rho_o = 5 \times 10^{23}\,\text{m}^{-3}$, $a = 1\,\text{nm}$ and crystal sizes $R = 34$–$78\,\text{nm}$. The simulations are shown at two different sample temperatures $T = 20, 50°\text{C}$.

As the temperature of the sample increases in Fig. 13b, the electron survival probability curves $P(t)$ become steeper and closer together, i.e. the recombination takes places faster.

2.5. Monte Carlo simulations of luminescence phenomena in nanodosimetric materials: excited state tunneling

TL signals from nanodosimetric materials have been studied extensively during the past twenty years, especially in the area of nanomaterials doped with rare earths. One of the primary effects being studied experimentally have been possible correlations between the nanocrystal size and the shape and magnitude of TL signals. While there is an abundance of experimental studies attempting to establish such correlations, the underlying mechanism is not well understood. In this section we present the simulations of TL glow curves by Pagonis and Truong [36], which are based on tunneling taking place from the excited state of the system.

In general, Fig. 14 shows three types of kinetic models which have been studied using Monte-Carlo methods. Fig. 14a shows the energy scheme in the well-known one trap one recombination center model (OTOR), which is commonly used to describe delocalized luminescence phenomena in crystalline solids ([1]). Several energy transitions are shown schematically: thermal or optical excitation of a carrier from the ground state of the electron trap into the conduction band (solid arrow D), retrapping from the conduction band into the trap (solid arrow T), and direct recombination transition of electrons from the conduction band into a recombination center (L) resulting in the emission of photons (dashed arrow R). It is noted

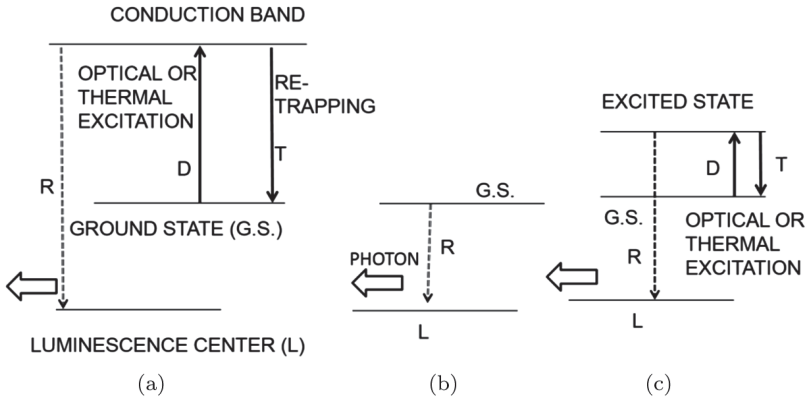

Fig. 14. (a) The energy scheme in the *delocalized* OTOR model, used for describing luminescence phenomena in crystalline solids. (b) The *localized* transition model for tunneling processes taking place from the ground state of the trap. (c) The *localized* transition model for tunneling processes taking place from the excited state of the trap. The various transitions are discussed in the text. (After Pagonis and Truong [36]).

that all transitions shown in Fig. 14a represent delocalized transition processes, as opposed to the models in Fig. 14b and Fig. 14c which are based on localized energy transitions. Previous TL Monte Carlo work based on Fig. 14a were presented in the papers by Mandowski and collaborators, and are summarized in Pagonis and Truong [36].

Typically the Monte Carlo calculations in Fig. 14a are performed with the total population of carriers simultaneously, and in each step of the Monte-Carlo simulation one finds the lowest transition time for all possible transitions, and this is the only transition which is executed. Mandowski and collaborators demonstrated how to perform Monte Carlo calculations in a solid consisting of a number of *separate* systems. Each transition in this scheme is represented mathematically by a transition rate $\lambda(t)(\mathrm{s}^{-1})$ as follows. The rate for thermal excitation (transition D) from the trap into the conduction band is $\lambda_{THERMAL}(t) = \mathrm{s}\exp(-E/kT)$ where E, s are the thermal activation energy and frequency factor characterizing the thermal properties of the electron trap. The corresponding optical excitation

rate (also transition D) is given by $\lambda_{OPTICAL} = \sigma I$ where σ (cm^2) is the optical cross section of the trap and I is the photon flux (*photons* $\mathrm{cm}^{-2}\,\mathrm{s}^{-1}$). The retrapping rate for transition T from the conduction band into the trap is given by the product $T = A_n(N - n)$ where n, N are the number of trapped electrons and total number of traps correspondingly, and A_n is the constant retrapping coefficient for a single carrier into a single trap. The recombination rate (transition R) from the conduction band into the luminescence center (L) is given by the product $R = A_m m$, where m is the number of trapped holes in recombination centers, and A_m is the constant recombination coefficient for a single carrier into a single center.

In each step of the Monte Carlo simulation, the times t_i of each allowed transition are generated for all carriers in the system, and can be evaluated from the integral equation (Mandowski and Świątek [24], their Eq. 5):

$$\int_0^{t_i} \lambda(t')dt' = -\ln(a_i) \tag{36}$$

where a_i is a homogeneous normalized random variable from the interval (0, 1) and $\lambda(t)$ (in s^{-1}) is the appropriate transition rate (T, R, or D) for the transition under consideration, as described above. Eq. (36) has simple analytical solutions for the transitions R, T in Fig. 14a, since these transitions do not depend on time. However, in the case of TL experiments Eq. (36) must be solved numerically, as described below.

Fig. 14b shows a ground state tunneling model which is based on localized energy transitions; recent Monte Carlo work using this type of model was presented in previous sections of this chapter.

In the third type of model shown in Fig. 14c, electrons can tunnel from the excited state of the electron trap to the luminescence center. During a typical laboratory experiment, one uses optical or thermal excitation, and the dominant process is the recombination process taking place from the excited state of the trapped electron to the recombination center. The relevant *localized* transitions are shown as D, T, R in Fig. 1c; although these transitions have some

mathematical similarity to the transitions of the delocalized model of Fig. 1a, the important difference is that they involve the excited state of the trap, instead of taking place via the conduction band.

In a typical TL experiment, the sample is heated with a linear heating rate $\beta(K/s)$ from a starting temperature T_o up to a high temperature around 500°C, so that the temperature varies with time t as $T(t) = T_o + \beta t$. Jain *et al.* [25] and previously Thioulouse *et al.* [9] and Chang and Thioulouse [37], demonstrated that for this type of experiment Eq. (36) must be replaced by the following Arrhenius type of expression (Jain *et al.* [34], their Eqs. 3 and 6):

$$\lambda(r,t) = s \exp[-r/a] \exp[-E/\{k_B(T_o + \beta t)\}] \tag{37}$$

where E is the thermal activation energy between the ground state and the excited state of the trapped electron, k_B is the Boltzmann constant and s is the frequency factor characterizing tunneling taking place from the excited state of the system. It is noted that Eq. (37) is derived by assuming quasi-static equilibrium conditions (QE) in the excited state tunneling model of Fig. 14c.

By combining Eqs. (36) and (37) we obtain:

$$s \exp[-r/a] \int_0^{t_i} \exp[-E/\{k_B(T_o + \beta t')\}] dt' = -\ln(a_i) \tag{38}$$

Pagonis and Truong [36] presented a Monte Carlo simulation study of the effect of nanocrystal size on the TL signals from a random distribution of electrons and positive ions, based on Eq. (38). These authors varied the following parameters in the model: the radius of the crystal R, the tunneling length a, and the relative concentrations of electrons and ions.

Typical results from the simulations of Pagonis and Truong [36] are shown in Fig. 15. As the radius of the nanocrystals becomes larger, the peaks of the TL glow curves shift towards lower temperatures and changes occur in both peak intensity and peak width. For large crystals with a constant density of positive ions, the TL glow curves reach the analytical limit expected for bulk materials.

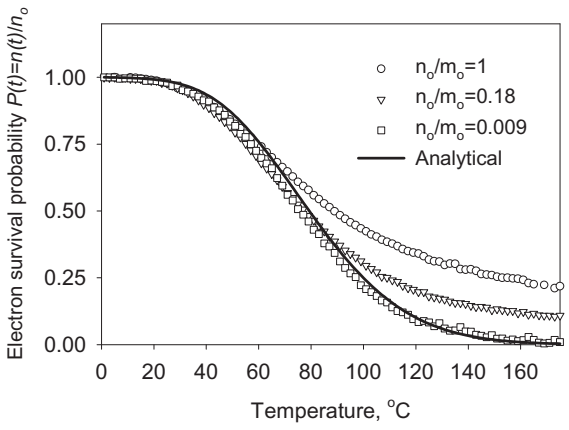

(a)

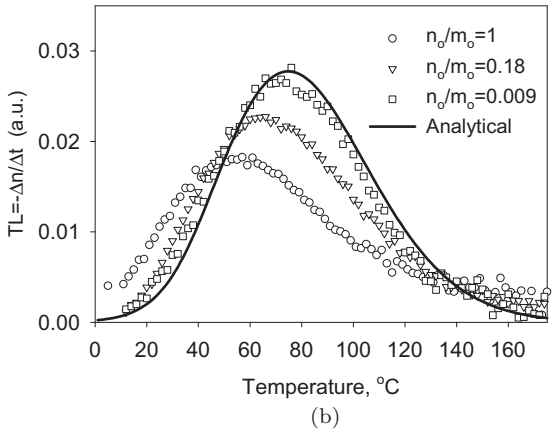

(b)

Fig. 15. Monte Carlo simulation for a spherical distribution, by varying the relative initial concentrations of electrons and positive ions in the system. The initial number of positive ions inside the sphere is kept constant at $m_o = 1100$, while the initial number of electrons is varied. The solid lines correspond to the analytical equation, which is valid for very low values of the ratio n_o/m_o. (a) The electron survival probability and (b) the corresponding TL glow curve (After Pagonis and Truong [36]).

Figure 16 shows simulations of TL glow curves in crystals with *equal* number of electrons and positive ions at all times. Figure 16a shows that at low temperatures the tunneling process for small crystals is *slower* than in large crystals, with the arrows indicating

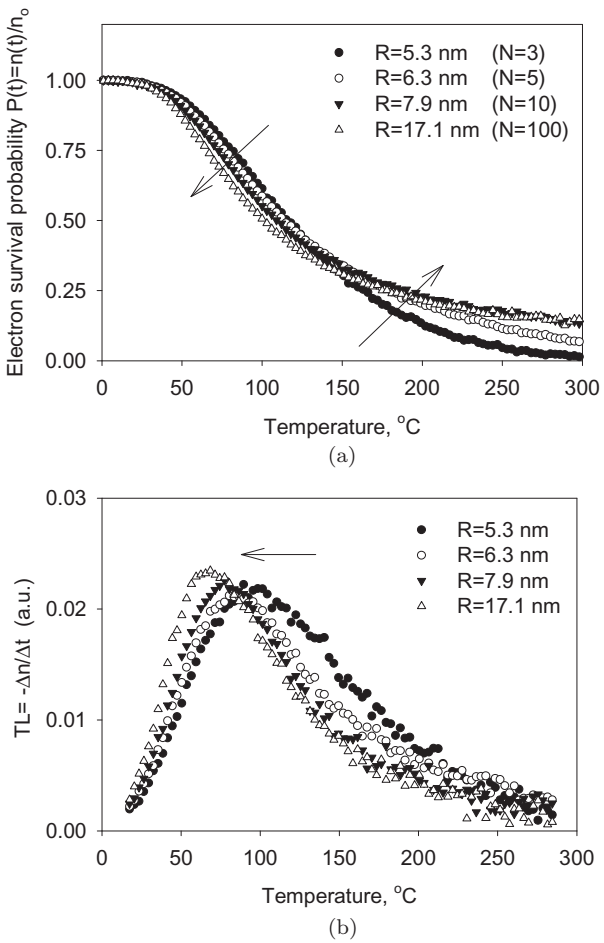

Fig. 16. Simulations for crystals with *equal* number of electrons and positive ions at all times. (a) At low temperatures the tunneling process for small crystals is *slower* than in large crystals, with the arrows indicating the direction of increasing radius R. At higher temperatures the order of the curves is reversed. (b) The corresponding simulated TL curves. (After Pagonis and Truong [36]).

the direction of increasing radius R. At higher temperatures the order of the curves is reversed. Fig. 16b shows the corresponding simulated TL curves.

Figure 17 shows the same type of simulations as Fig. 16, for a smaller tunneling length $a = 1\,\text{nm}$ while keeping all the other

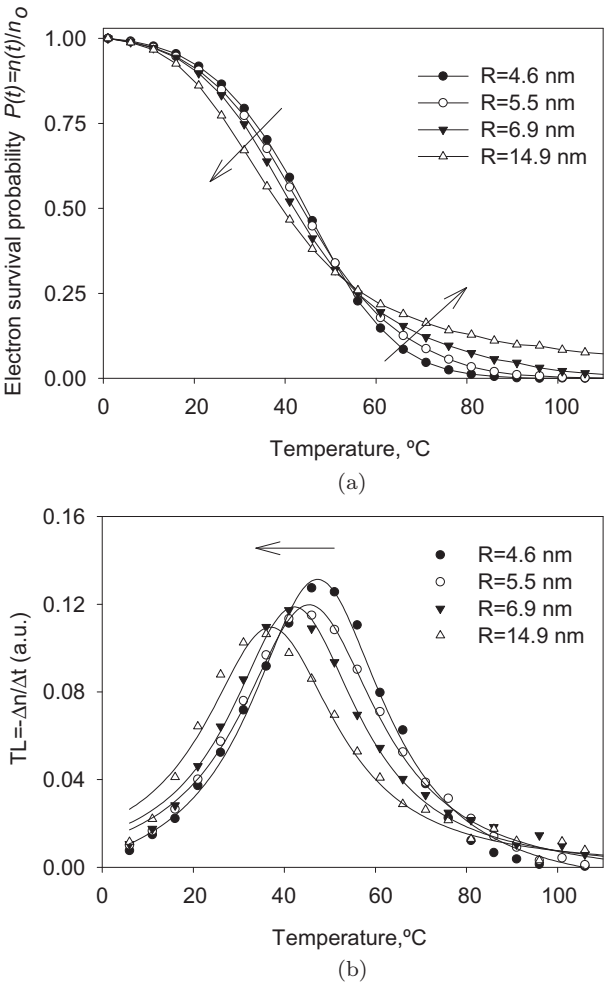

Fig. 17. The simulations in Fig. 16 are repeated for a smaller tunneling length. The TL height shows the opposite behavior than in Fig. 16b. (After Pagonis and Truong [36]).

parameters fixed. The TL height as a function of the radius R in Fig. 17 shows the opposite behavior than the corresponding curves in Fig. 16. The solid lines are again a guide to the eye.

As the radius of the nanocrystals becomes larger, the peaks of the TL glow curves shift towards lower temperatures and changes

occur in both peak intensity and peak width. For large crystals with a constant density of positive ions, the TL glow curves reach the analytical limit expected for bulk materials.

Pagonis and Truong [36] compared the results from the Monte Carlo simulations with experimental data for Durango apatite, a material which is known to exhibit strong anomalous fading due to tunneling. Specifically Polymeris *et al.* [38] found that ball milling of Durango apatite powders for up to 48 hours, resulted in significant changes in the TL and OSL luminescence signals in this material. Figure 18 shows some of their experimental TL glow curves for the same Durango apatite sample which has undergone ball milling for 2 hours (dark circles) and 24 hours (open circles). The sample was irradiated with a small test dose after the end of the ball milling process, and its prompt TL signal was measured immediately after. Figure 18a shows the complete normalized TL glow curves for the two ball milling times, while Fig. 18b shows details of the same data between 200 and 400°C. The main peak in the TL glow curve for the smaller crystals with an average grain size $R = (0.4 \pm 0.2)\mu$m, is shifted towards higher temperatures than the TL for larger crystals with average grain size $R = (5.0 \pm 1.0)\mu$m. The *qualitative* behavior of the TL glow curves in Fig. 18 is very similar to the simulated behavior shown in Fig. 17, although the temperature and radius scales are very different. The grain sizes in Polymeris *et al.* [38] were obtained by analyzing scanning electron microscope images (SEM) of the ball milled sample. This comparison of experimental data with the Monte Carlo model in this chapter is very encouraging, and prompts the need for additional work to produce quantitative agreement between experiment and theory.

Pagonis and Truong [36] also examined the commonly used assumption of nearest neighbor interactions within the model, and presented simulated examples at very high charge densities, in which this assumption breaks down. Finally these authors also demonstrated that the Monte Carlo method presented in their paper can also be used for linearly modulated infrared stimulated luminescence (LM-IRSL) signals, which are of importance in luminescence dosimetry and luminescence dating applications.

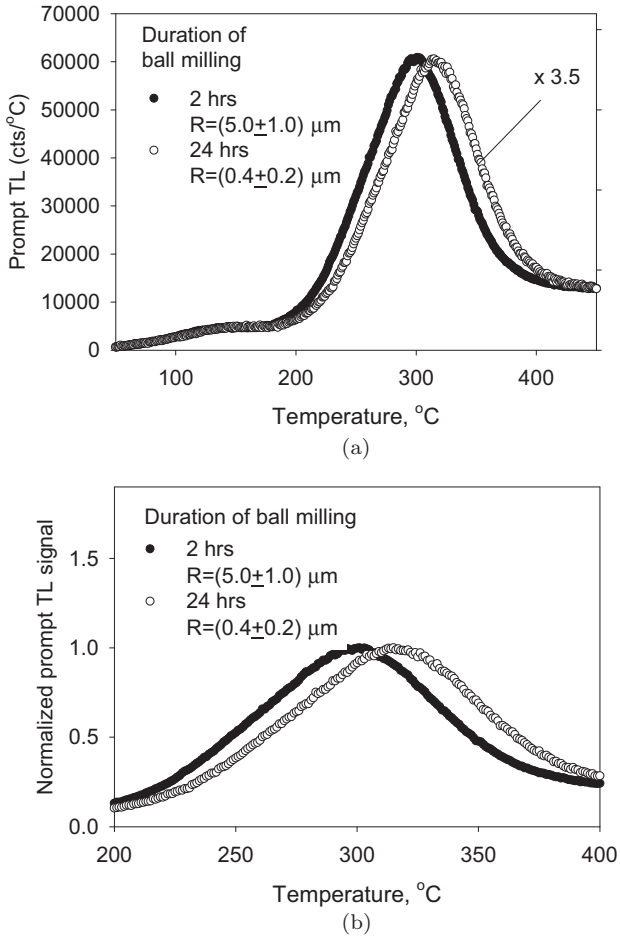

Fig. 18. Experimental TL glow curves for a Durango apatite sample which has undergone ball milling for 2 hours (dark circles, larger crystals) and 24 hours (open circles, smaller crystals). (a) The complete TL glow curves (b) Detailed view of the normalized signals from (a), between 200 and 400°C. (After Pagonis and Truong [36] and Polymeris *et al.* [38]).

2.6. Conclusions

In this chapter, two approaches were discussed for calculating tunneling phenomena in random distributions of electrons and positive ions. The differential equation approach is useful for large crystals, and

several analytical equations are available in the literature. Several of these analytical equations have been developed by assuming that the concentrations of electrons is much smaller than the concentration of positive ions, which allows the system to be described by the constant density of positive ions. The model by Jain *et al.* [10] and the analytical equations developed by Kitis and Pagonis [11] have been a major recent development, and have contributed in the understanding of tunneling phenomena in a random distribution of electron-hole pairs. Specifically the analytical equations by Kitis and Pagonis [11] have now been used to describe luminescence signals from a variety of feldspars and apatites (Polymeris *et al.* [39]; Sahiner *et al.* [40]; Sfampa *et al.* [41]; Kitis *et al.* [42]).

The Monte Carlo approach is useful for crystals of any size, especially in cases where analytical equations are not available in the literature. The rate of quantum tunneling in random distributions of electrons and positive ions was shown to depend in a complex manner on three fundamental lengths in the system: the radius of the crystal R, the tunneling length a, and the initial average distance $\langle d \rangle$ between electrons and positive ions (which is directly related to the density of charges in the material).

Both the differential equation and Monte Carlo approaches can be used to describe the ground state tunneling phenomena, as well as tunneling taking place from the excited state of the electron trap. Further modeling work will need to combine the localized transition models in this chapter with delocalized transitions involving the conduction and valence band, as well as transitions taking place via the band tail states.

References

[1] R. Chen and V. Pagonis, 2011. *Thermally and Optically Stimulated Luminescence: A Simulation Approach* (Chichester: Wiley and Sons).

[2] V. Pagonis, R. Chen, C. Kulp and G. Kitis, "An overview of recent developments in luminescence models with a focus on localized transitions," *Radiat. Meas.*, vol. 106, pp. 3–12, 2017.

[3] N. Salah, "Nanocrystalline materials for the dosimetry of heavy charged particles: A review," *Radiat. Phys. Chem.*, vol. 80, pp. 1–10, 2011.

[4] H.T. Sun and Y. Sakka, "Luminescent metal nanoclusters: Controlled synthesis and functional applications," *Sci. Technol. Adv. Mater.*, vol. 15, p. 014205, 2014.

[5] I. Eliyahu, Y.S. Horowitz, L. Oster, S. Druzhyna and I. Mardor, "Nanodosimetric kinetic model incorporating localized and delocalized recombination: Application to the prediction of the electron dose response of the peak 5a/5 ratio in the glow curve of LiF:Mg,Ti (TLD-100)," *Radiat. Meas.*, vol. 71, pp. 226–231, 2014.

[6] M. Tachiya and A. Mozumder, "Decay of trapped electrons by tunnelling to scavenger molecules in low temperature glasses," *Chemical Physics Letters*, vol. 28, pp. 87–89, 1974.

[7] B. Li and S.H. Li, "Investigations of the dose-dependent anomalous fading rate of feldspar from sediments," *J. Phys. D: Appl. Phys.*, vol. 41, p. 225502, 2008.

[8] P. Avouris and T.N. Morgan, "A tunneling model for the decay of luminescence in inorganic phosphors: The case of Zn_2SiO_4:Mn," *J. Chem. Phys.*, vol. 74, p. 4347, 1981.

[9] P. Thioulouse, E.A. Giess and I.F. Chang "Investigation of thermally stimulated luminescence and its description by a tunneling model," *J. Appl. Phys.*, vol. 53, p. 9015, 1982.

[10] M. Jain, B. Guralnik and M.T. Andersen, "Stimulated luminescence emission from localized recombination in randomly distributed defects," *J. Phys.: Condens. Matter*, vol. 24, 385402 (12pp), 2012.

[11] G. Kitis and V. Pagonis, "Analytical solutions for stimulated luminescence emission from tunneling recombination in random distributions of defects," *J. Lumin.*, vol. 137, pp. 109–115, 2013.

[12] V. Pagonis and G. Kitis, "Mathematical aspects of ground state tunneling models in luminescence materials," *J. Lumin.*, vol. 168, pp. 137–144, 2015.

[13] V. Pagonis, H. Phan, D. Ruth and G. Kitis, "Further investigations of tunneling recombination processes in random distributions of defects," *Radiat. Meas.*, vol. 58, pp. 66–74, 2013.

[14] V. Pagonis, C. Kulp, C. Chaney and M. Tachiya, "Quantum tunneling recombination in a system of randomly distributed trapped electrons and positive ions," *J. Phys. Condens. Matter*, vol. 29, no. 36, p. 365701, 2017, 2017c.

[15] V. Pagonis, S. Bernier, F.M. Vieira and S. Steele, "The effect of crystal size on tunneling phenomena in luminescence dosimetric materials," Accepted at *Nucl. Instr. Methods B*, 2017.

[16] D.J. Huntley and O.B. Lian, "Some observations on tunnelling of trapped electrons in feldspars and their implications for optical dating," *Quat. Sci. Rev.*, vol. 25, p. 2503, 2006.

[17] V. Pagonis and C. Kulp "Monte Carlo simulations of tunneling phenomena and nearest neighbor hopping mechanism in feldspars," *J. Lumin.*, vol. 81, pp. 114–120, 2017.

[18] B. Guralnik, B. Li, M. Jain, R. Chen, R.B. Paris, A.S. Murray, S.H. Li, V. Pagonis, P.G. Valla and F. Herman, "Radiation-induced growth and

isothermal decay of infrared-stimulated luminescence from feldspar," *Radiat. Meas.*, pp. 224–23, 2015.

[19] V. Pagonis, E. Gochnour, M. Hennessey and C. Knower, "Monte Carlo simulations of luminescence processes under quasi-equilibrium (QE) conditions," *Radiat. Meas.*, vol. 67, pp. 67–76, 2014.

[20] R.N. Kulkarni, "The development of the Monte Carlo method for the calculation of the thermoluminescence intensity and the thermally stimulated luminescence," *Radiat. Prot. Dosim.*, vol. 51, pp. 95–105, 1994.

[21] A. Mandowski, "Modelling of charge carriers' transport and trapping phenomena in one-dimensional structures during thermal stimulation," *J. Electr.*, vols. 51-51, pp. 585–589, 2001.

[22] A. Mandowski, "Calculation and properties of trap structural functions for various spatially correlated systems," *Radiat. Prot. Dosim.*, vol. 119, pp. 85–88, 2006.

[23] A. Mandowski, "How to detect trap cluster systems?" *Radiat. Meas.*, vol. 43, pp. 167–170, 2008.

[24] A. Mandowski and J. Świątek, "Monte Carlo simulation of thermally stimulated relaxation kinetics of carrier trapping in microcrystalline and two-dimensional solids," *Phil. Mag. B*, vol. 65, pp. 729–732, 1992.

[25] A. Mandowski and J. Świątek, "On the influence of spatial correlation on the kinetic order of TL," *Radiat. Prot. Dosim.*, vol. 65, pp. 25–28, 1996.

[26] A. Mandowski and J. Świątek, "Thermoluminescence and trap assemblies — results of Monte Carlo calculations," *Radiat. Meas.*, vol. 29, pp. 415–419, 1998.

[27] A. Mandowski and J. Świątek, "The kinetics of trapping and recombination in low dimensional structures," *Synth. Metals*, vol. 109, pp. 203–206, 2000.

[28] V. Pagonis and G. Kitis, "Prevalence of first order kinetics in thermoluminescence materials: An explanation based on multiple competition processes," *Phys. Status Solidi B*, pp. 1–12, 2012.

[29] V. Pagonis, R. Chen and G. Kitis, "On the intrinsic accuracy and precision of luminescence dating techniques for fired ceramics," *J. of Arch. Science*, vol. 38, pp. 1591–1602, 2011.

[30] Adamiec, "Investigation of a numerical model of the pre-dose mechanism in quartz," *Radiat. Meas.*, vol. 39, pp. 175–189, 2005.

[31] G. Adamiec, A. Bluszcz, R. Bailey and M. Garcia-Talavera, "Finding model parameters: Genetic algorithms and the numerical modelling of quartz luminescence," *Radiat. Meas.*, vol. 41, pp. 897–902, 2006.

[32] V. Pagonis and R. Chen, "Monte Carlo simulations of TL and OSL in nanodosimetric materials and feldspars," *Radiat. Meas.*, vol. 81, pp. 262–269, 2015.

[33] A. Larsen, S. Greilich, M. Jain and A.S. Murray, "Developing a numerical simulation for fading in feldspar," *Radiat. Meas.*, vol. 44, p. 467, 2009.

[34] M. Jain, R. Sohbati, B. Guralnik, A.S. Murray, M. Kook, T. Lapp, A.K. Prasad, K.J. Thomsen and J.P. Buylaert, "Kinetics of infrared stimulated luminescence from feldspars," *Radiat. Meas.*, vol. 81, pp. 242–250, 2015.

[35] G.S. Polymeris, V. Pagonis and G. Kitis, "Thermoluminescence glow curves in preheated feldspar samples: An interpretation based on random defect distributions," *Radiat. Meas.*, vol. 97, pp. 20–27, 2017.

[36] V. Pagonis and P. Truong, "Thermoluminescence due to tunneling in nanodosimetric materials: A Monte Carlo study," *Physica B: Condensed Matter*, vol. 531, pp. 171–179, 2018.

[37] I.F. Chang and P. Thioulouse, "Treatment of thermostimulated luminescence, phosphorescence, and photostimulated luminescence with a tunneling theory," *J. Appl. Phys.* vol. 53, p. 5873, 1982.

[38] G.S. Polymeris, I.K. Sfampa, M. Niora, E.C. Stefanaki, L. Malletzidou, V. Giannoulatou, V. Pagonis and G. Kitis, "Anomalous fading in TL, OSL and TA – OSL signals of Durango apatite for various grain size fractions; from micro to nano scale," *J. Lumin.*, vol. 195, pp. 216–224, 2018.

[39] G.S. Polymeris, V. Giannoulatou, I.K. Sfampa, N.C. Tsirliganis and G. Kitis, "Search for stable energy levels in materials exhibiting strong anomalous fading: The case of apatites," *J. Lumin.*, vol. 153, pp. 245–251, 2014.

[40] E. Şahiner, G. Kitis, V. Pagonis, N. Meriç and G.S. Polymeris, "Tunnelling recombination in conventional, post-infrared and post-infrared multi-elevated temperature IRSL signals in microcline K-feldspar," *J. Lumin.*, vol. 188, pp. 514–523, 2017.

[41] I.K. Sfampa, G.S. Polymeris, N.C. Tsirliganis, V. Pagonis and G. Kitis, "Prompt isothermal decay of thermoluminescence in an apatite exhibiting strong anomalous fading," *Nucl. Instr. Meth. B*, vol. 320, pp. 57–63, 2014.

[42] G. Kitis, G.S. Polymeris, I.K. Sfampa, M. Prokic, N. Meriç and V. Pagonis, "Prompt isothermal decay of thermoluminescence in MgB_4O_7:Dy,Na and LiB_4O_7:Cu," *In dosimeters. Radiat. Meas.*, vol. 84, pp. 15–25, 2016.